water

MDPI

Article

Study on the Instability Activation Mechanism and Deformation Law of Surrounding Rock Affected by Water Immersion in Goafs

Sihai Yi [1], Yu Zhang [1,*], Haiyang Yi [2], Xueliang Li [3], Xu Wang [1] and Yun Wang [1] and Tingxiang Chu [2]

[1] School of Safety Engineering, North China Institute of Science and Technology, Beijing 101601, China
[2] School of Mine Safety, North China Institute of Science and Technology, Beijing 101601, China
[3] China Coal Science and Technology Ecological Environment Technology Co., Ltd., Beijing 100013, China
* Correspondence: 15932266905@163.com

Abstract: Large-scale goafs are left after coal seam mining. Due to the low-lying terrain, the goaf will be filled and soaked by groundwater, which may lead to instability of the remaining coal pillars in the goaf and cause uneven settlement of the overlying rock. Consequently, there may be overlying rock movement and surface subsidence, which endangers the safety of the building (structure) above the goaf. Considering the strip goaf of Dai Zhuang coal pillar as an example, this study investigated the evolution of instability and deformation of surrounding rocks affected by water immersion using the similar material simulation test method. The results of the study reveal that under the effect of prolonged water immersion in the goaf, the damage to the coal pillar in the strip underwent a stagewise evolution process of several instances of creep damage at the edge of coal pillar followed by overall destabilization damage, and the overburden movement revealed stage characteristics of small step subsidence several times followed by sudden large subsidence. Furthermore, based on Wilson's coal pillar instability theory, the instability mechanism of the strip coal pillar under the action of water immersion was found to be triggered by the reduced strength of the coal pillar from the effect of water immersion, the continuous creep damage to the strip coal pillar from outside to inside, and the continuous shortening of the elastic zone of the coal pillar until its bearing capacity was lower than the load it was carrying. The research results are expected to serve as theoretical guidance for the study of coal pillar stability and the development and utilization of surface construction above goafs.

Keywords: goaf; water immersion; physical simulation; instability mechanism; movement; deformation

Citation: Yi, S.; Zhang, Y.; Yi, H.; Li, X.; Wang, X.; Wang, Y.; Chu, T. Study on the Instability Activation Mechanism and Deformation Law of Surrounding Rock Affected by Water Immersion in Goafs. *Water* **2022**, *14*, 3250. https://doi.org/10.3390/w14203250

Academic Editor: Dan Ma

Received: 29 July 2022
Accepted: 13 October 2022
Published: 15 October 2022

1. Introduction

After coal mining, large-scale goafs are left behind, forming poor foundations. These goafs are in a relatively stable state for a short period of time after the underground mining stops. However, the influence of external factors may subsequently result in destabilization of the residual coal (rock) pillar in the goaf, causing uneven subsidence of overlying rock and surface movement, which is a major safety hazard for surface land use and building development above the goaf.

Coal pillar stability is crucial for maintaining safety and stability in the surrounding rocks in goafs. Many scholars have investigated the failure characteristics and failure mechanism of residual coal (rock) pillars in goafs. It is considered that the stability of residual coal pillars in the mining area may be influenced by a number of external factors. Among these, larger seismic or impact loading effects are highly likely to cause damage to the coal rock, resulting in settlement of the overburden rock in the mined area.

Yan et al. [1] studied the damage mechanism of rock masses under the action of earthquakes based on the Moore–Coulomb criterion and fluctuation theory. The dynamic loads generated by earthquakes change the original stable stress field of the rock mass and the intensity of the seismic waves exceeds the ultimate strength of the rock mass, so the rock mass will be damaged, leading to destabilization of the mining area. Cao et al. [2] analyzed the mechanism of coal rock impact damage by mine earthquakes based on energy and stiffness theory, in which the propagation of vibration wave energy into the mined area causes the coal rock system to gather a large amount of elastic strain energy and become unstable. Xue et al. [3] studied the mechanism of coal pillar bursting in terms of energy evolution, in which vertical stress concentration and elastic strain energy accumulation occur during mining, and rock bursts occur with the sudden release of elastic deformation energy retained in the coal pillar during backfill mining, leading to destabilization of the mined area. Maleki et al. [4], through long-term observations of coal mines, showed that horizontal stresses build up in coal pillars and the unstable release of strain energy is much greater than the capacity of the internal support system of the pillar, leading to destabilization of the mining area. Deng et al. [5] investigated the dynamic yielding mechanism of rock bursts in coal pillars during underground mining, and they identified sinusoidal stress waves as a major influence on the occurrence of rock bursts by dynamic stimulation loads, which are an important factor affecting the stability of the mining area. In addition, the mining method affects coal pillar stability. Xia et al. [6] studied the dynamic evolution characteristics of the vertical stress and plastic state of coal pillars under repetitive mining, and they observed that the transition from the elastic to the plastic state of coal pillars will lead to large deformation and damage, resulting in destabilization of the mined area. Rashed et al. [7] analysed the factors affecting pillars in multi-stage coal seam mining, where the distribution of coal pillar offsets produces an asymmetric stress distribution and high stress concentrations can lead to local instability in the mined area. Lan et al. [8] investigated the deformation mechanism of deep strip coal pillars, in which strip mining caused stress concentration inside the coal pillars, and the shear force at the edge of the coal pillars caused by the main stress difference was located on the Moore–Coulomb yield surface, leading to destabilization of the coal pillars.

Among the many influencing factors, water immersion in a goaf is one of the important external influencing factors [9–12]. Aiting et al. [13] investigated the changes in water absorption characteristics and pore structure of coal samples based on water immersion time via nuclear magnetic resonance and scanning electron microscopy. They examined the deformation and damage characteristics of coal samples under different water immersion cycles through uniaxial compression experiments. Yao et al. [14] analyzed the stability of coal pillars and surrounding rocks under the action of water through physical experiments to investigate the destabilization mechanism of coal samples. They found that the strength and fracture development characteristics of coal rocks were closely related to the water content.

Numerous scholars [15–17] have studied the characteristics of overburden settlement changes by analyzing the mechanism of rock damage. Poulsen et al. [18] quantified the effect of changes in intensity of different lithological components in coal pillars subjected to water immersion on the stability state of the coal pillar. Dai et al. [19] studied an intelligent method of identifying the stability of coal pillars in cross-section and analyzed the load transfer law of each overlying rock layer of the pillars. Castellanza et al. [20–23] proposed a method for evaluating the stability of coal pillars in mines based on different influencing factors under external conditions. Chen et al. [24] determined the long-term bearing capacity distribution pattern of strip coal pillars based on a field test. Liu et al. [25] established a coal pillar stability evaluation model based on the characteristics of coal pillar damage and limit equilibrium theory.

Numerous studies have investigated the influence of the stress distribution characteristics of coal pillars and their stability and damage law during mining through theoretical analysis and numerical simulation [26–31]. Most of these studies employed

mechanical tests of coal samples to deduce the mechanical mechanism of coal pillar instability in goafs. However, mechanical tests of coal samples cannot simulate the environmental working conditions of actual coal pillars. Moreover, the size and shape of coal samples have an effect on the mechanics, limiting the research results obtained, which cannot be applied to actual engineering.

To reflect a more realistic destabilization evolution process of coal and rock body affected by water immersion in strip goafs, we conducted experimental research on the destabilization activation mechanism and deformation law of the surrounding rock. A physical simulation test was conducted by replicating the environmental working conditions of actual projects. The research results are expected to serve as theoretical guidance for the study of coal pillar stability and the development and utilization of surface construction above goafs.

2. Engineering Geology Background

Daizhuang coal mine is located in Jining City, Shandong Province, China (Figure 1), with mining coal seams 3 $_{up\,1}$, 3 $_{up}$, 3 $_{down}$, 6, 15 $_{up}$, 16, and 17. The coal mine has a well field area of 65.6257 km^2, mining depth of 200–1000 m, and production scale 1.5 million tons/year, and is valid for 40 years.

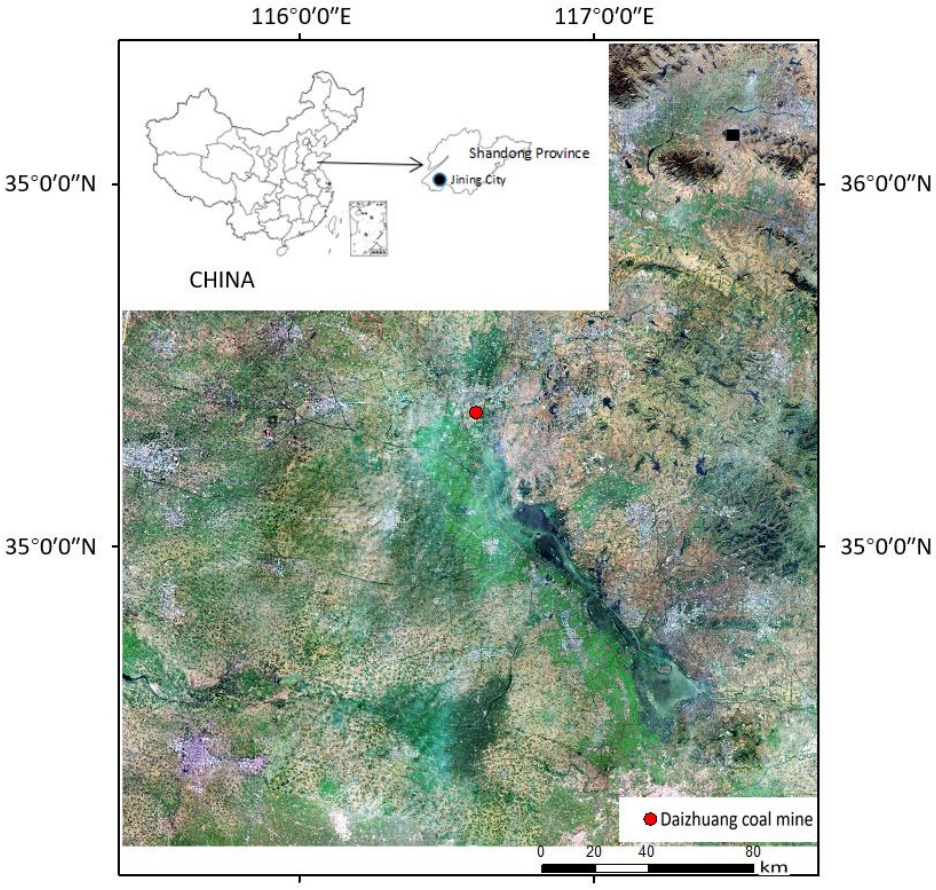

Figure 1. Mineral location map.

The stratigraphic development in the area includes Ordovician, Carboniferous, Permian, Jurassic, and Quaternary, in order from oldest to newest (Figure 2). The overlying bedrock of the mined coal seam is primarily composed of sandstone, mudstone, sandy mudstone, and sand conglomerate. The loose layer of the fourth series is relatively thick, with an average thickness of 245 m, primarily composed of clay, sandy clay, clayey sand, sand, and sand conglomerate layers. The terrain in the well field is flat, and is a recently

formed alluvial plain. The faults in the well field are relatively developed, predominantly in three directional groups: northeast, near-north–south, and northwest. The primary aquifers in the area are a fourth series loose aquifer and an Ordovician tuff karst aquifer. The main coal-bearing strata in this field are Shanxi and Taiyuan Groups. Since the mine began operation in 2000, predominantly 3 up and 3 down coal seams have been mined. The coal seams have been explored through single-level vertical shafts. The method of coal mining is to progress toward the long wall and backward, with comprehensive mechanized technology and a collapse method employed to manage the roof.

era	period	group	formation	min-max / The average thickness (m)	Lithological description
Cenozoic Era	Quaternary Period			96.3～412.87 / 245.75	It consists of layers of clay, sandy clay, clayey sand, sand and gravel.
Mesozoic Era	Jurassic Period	Zibo group	Santai Group J_3s	Maximum residual thickness 358.40	It is mainly composed of clay, sandy clay, clayey sand, sand and gravel layers.
Palaeozoic Era	Permian Period	Shihezi Group $P_{2-3}\hat{S}$		0.00～371.45 / 288.00	The upper part is mainly composed of yellow-green, gray, purple-red and other variegated mudstone, siltstone and gray-green sandstone; the middle part is composed of mudstone and quartz sandstone; the lower part is mainly composed of yellow-green, gray-green, gray, purple and other variegated mudstone, siltstone, Grey-green sandstone composition.
		Yuemengou Group C_2-P_1Y	Shanxi Group $P_{1-2}\hat{S}$	57.80～114.70 / 75.57	It is mainly composed of light gray, gray-white and gray-green sandstone, dark gray, gray-black siltstone, mudstone and coal seam. The main coal-bearing strata in this mine field have 4 coal-bearing layers (2, 3 upper, 1, 3 upper and 3 lower coal seams), and the mineable coal seams are 3 upper 1, 3 upper and 3 lower coal seams.
	Carboniferous Period		Taiyuan Group C_2P_1t	167.10～212.26 / 184.42	It is mainly composed of dark gray, gray-black siltstone, mudstone, gray to gray-white siltstone, fine sandstone, limestone and coal seams. Contains 14 layers of limestone. There are 24 coal-bearing layers (4-20 coal seams), and 4 coal seams (6, 15 upper, 16 upper, and 17 coal seams) which can be mined and partially mined.
			Benxi Group C_2b	2.20～23.74 / 9.58	It is mainly composed of gray, gray-green, dark gray claystone and siltstone.
	Ordovician Period	Majiagou Group $O_{2-3}M$		＞800	The maximum exposed thickness in the mine field is 177.84m. Mainly gray-white and brown-gray thick-layered dolomitic limestone, leopard-skin limestone, intercalated with marl and calcareous mudstone.

Figure 2. Stratigraphy infographic.

The aquifers affecting the mine production, from top to bottom, mainly include the Quaternary sand and gravel pore aquifer, Shanxi Formation sandstone fissure aquifer (group), the 3 limestone karst fissure aquifer, the 10 down limestone karst fissure aquifer, the 13 limestone karst fissure aquifer, and the Ordovician limestone karst fractured aquifer.

(1) The Quaternary sand and gravel pore aquifer is divided into two groups, upper and lower. The upper group has an average thickness of 104.20 m, with lithology mainly consisting of medium- and coarse-grained quartz sand layers and clayey sand, and the water chemistry type is HCO_3-Ca·Mg or HCO_3-Ca·K+Na, with strong water richness; the lower group has an average thickness of 65.90 m, with lithology mainly consisting of clayey feldspar and quartz gravel layers, and the water chemistry type is SO_4·HCO_3-Ca·K+Na, with medium water richness.

(2) The sandstone fissure aquifer of the Shanxi Group is a direct water-filled aquifer for mining the 3 up and 3 down coal seams, with an average thickness of 75.57 m. The lithology is mainly medium-, coarse-, and fine-grained sand layers, and the water chemistry type is SO_4·HCO_3-K+Na, with medium water richness.

(3) The 3 limestone karst fissure aquifer has an average thickness of 5.69 m and a water chemistry type of SO_4·HCO_3-K+Na with moderate and highly heterogeneous water enrichment.

(4) The 10 lower limestone karst fissure aquifer, which is at the roof of the 16 coal seam, is a direct water-filled aquifer for mining the 16 coal seam, with an average thickness of 5.32 m and a water chemistry type of SO_4·HCO_3-Ca·K+Na.

(5) The 13 limestone karst fissure aquifer has an average thickness of 5.60 m and water chemistry type SO_4-Ca·Mg, with medium water richness.

(6) In the Ordovician limestone karst fissure aquifer, most of the boreholes exhibit a thickness of about 50 m, and the water chemistry type is SO_4·HCO_3-Ca·Mg and SO_4·HCO_3-Ca, with medium water richness.

The study area is a coal mining area under pressure in the village; there are 3 $_{up}$ coal seams with a thickness of 2.6 m, an approximately horizontal dip angle, and average mining depth of 550 m, with an overlying Quaternary rock layer approximately 300 m thick and bedrock approximately 250 m thick. The area was mined by strip mining, mining strip width of 50 m, leaving strip width of 100 m. Three strip faces were mined in sequence from 12 October to 27 December 2013, from 5 February to 16 May 2014, and from 7 May to 8 June 2014. The strip-mining schematic is shown in Figure 3. From 12 to 20 September 2018, exploration of the goaf was carried out using the transient electromagnetic method, and the results showed a significant anomalous low-resistance strip-like response at all three working face locations, suggesting an electrical reflection of water accumulation in the goaf, where the goaf should have been full of water.

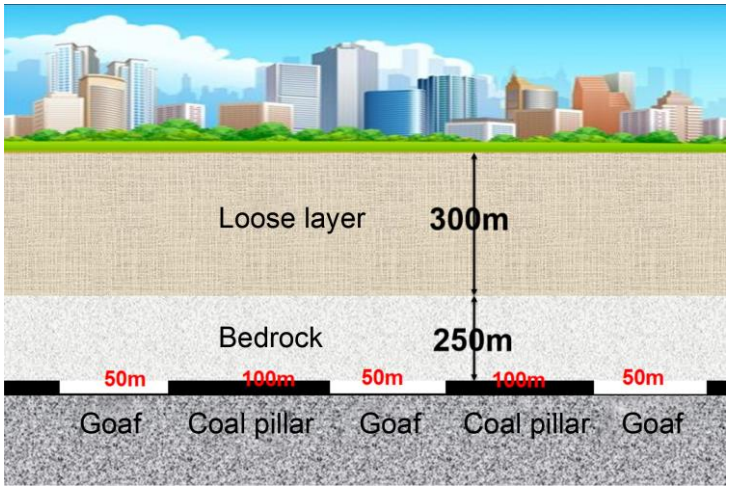

Figure 3. Schematic diagram of strip mining in Daizhuang coal mine.

3. Physical Simulation Experiment of Water Immersion in Mining Area

3.1. Model Design

Simulation experiments were conducted using a two-dimensional (2D) similar simulation table with a size of 2000 mm × 300 mm × 1800 mm (L × W × H). Considering the similarity theorem and related similarity criterion, the geometric similarity constant of the model was selected as 1:150 and was combined with the geological mining conditions in the simulated study area. However, restricted by the height of the model frame and geometric similarity constants, the experiment could not simulate the full profile of the overlying rock layer; thus, gravity load compensation was applied to the overlying rock (soil) layer that could not be simulated by the model. The gravity compensation load was calculated to be approximately 24.2 kPa. The design of the experimental simulation model is shown in Figure 4.

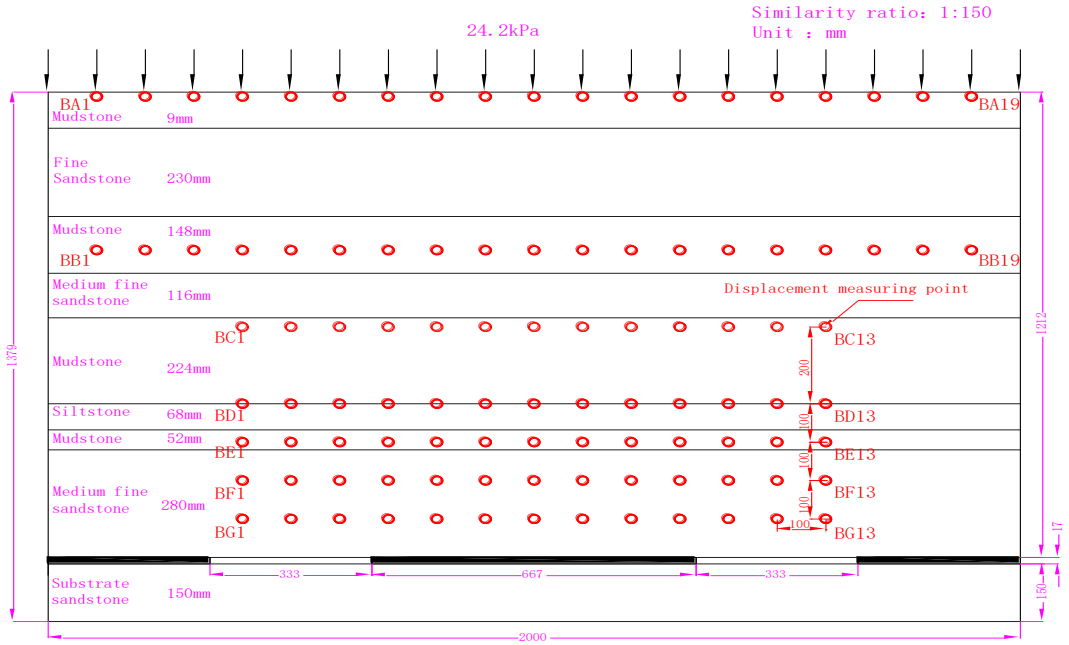

Figure 4. Experimental model design.

3.2. Material Proportioning

Similar simulated materials include river sand as aggregate, gypsum and calcium carbonate as binder, and mica flakes as layering material. Considering that water accumulation in the goaf changes the mechanical properties of similar materials, appropriate water-blocking additives must be added to the binder, and the softening law of coal pillar strength with water immersion time was determined through proportioning tests. Thus, 5% of total weight of petroleum jelly was proposed as a water-blocking additive. The specific mechanical parameters of the rock formation and its model stratification and proportioning are listed in Table 1.

Table 1. Main mechanical and proportioning parameters of rock formations [32].

Serial Number	Rock Layer	Layer Thickness (m)	Compressive Strength (MPa)	Test Weight (t/m³)	Matching Number	Material Weight (kg)				
						River Sand	Plaster	Calcium Carbonate	Water-Blocking Additive	Water
10	Mudstone	14.1	31.6	2.65	1028	82.04	1.64	6.56	4.51	9.02
9	Fine sandstone	34.5	67.8	2.57	1055	200.73	10.04	10.04	11.04	22.08
8	Mudstone	22.2	31.6	2.65	1028	129.16	2.58	10.33	7.10	14.21
7	Medium-fine sandstone	17.4	64.8	2.55	1055	101.24	5.06	5.06	5.57	11.14
6	Mudstone	33.6	31.6	2.65	1028	195.49	3.91	15.64	10.75	21.50
5	Siltstone	10.2	64.0	2.60	1055	59.35	2.97	2.97	3.26	6.53
4	Mudstone	7.8	31.6	2.65	1028	45.38	0.91	3.63	2.50	4.99
3	Medium-fine sandstone	42	64.8	2.55	1055	244.36	12.22	12.22	13.44	26.88
2	3_{up} coal	2.6	18.5	1.40	1037	15.13	0.45	1.06	0.83	1.66
1	Fine sandstone	22.5	67.8	2.57	1055	130.91	6.55	6.55	7.20	14.40

3.3. Displacement Observation Scheme

The experiment was primarily conducted to observe the displacement of the rock seam. Strain monitoring was carried out by using the ISM-CONTR-VG5-2DB series non-contact video strain displacement precision measurement system (Imetrum, UK) (Figure 5). The system uses a camera to collect surface images of a specimen during the deformation process, and it uses speckle recognition technology to accurately track the movement between points on the measured object. A patented sub-pixel image recognition algorithm was used to perform ultra-high-resolution strain, rotation, and displacement measurements. It supports a measurement range up to 100 m, a maximum distance of 1000 m, and 2D displacement resolution of 0.01 mm within 10 m. Seven measurement lines (Figure 4) were designed and arranged in the rock seam, and the distance to the coal seam from the top to the bottom of each measurement line was 1200, 800, 600, 400, 300, 200, and 100 mm, numbered as lines BA, BB, BC, BD, BE, BF, and BG, respectively. The distance between measurement points of each line was 100 mm.

After the model was dried and finalized, waterproof observation points were arranged on the surface according to the measurement point arrangement chart. The measurement points facilitate mobile monitoring of the entire process of similar model strip mining and water immersion experiments in extraction goaf s, using the photogrammetry monitoring system to obtain rich displacement data. The 2D displacement resolution of the photogrammetric monitoring system was 0.01 mm within 10 m.

Figure 5. Non-contact video strain displacement precision measurement system.

4. Overlying Rock Movement and Deformation Law

4.1. Strip Mining Overburden Movement and Deformation Law

Once the model layout was completed and the model was dried and set, strip mining was performed according to the experimental requirements.

After the strip working face was mined, the roof rock layers on the left and right sides of the strip working face fell and fractured one after the other. Subsequently, two fracture zones developed independent of each other; the overlying rock developed into medium-grained sandstone, and the height of the fracture zone was approximately 15 m. The fracture zone had an approximately trapezoidal outline, and a stress arch was formed above it. The stress arch supported most of the self-weight load of the overburden rock above, controlled its movement and deformation, and transferred its stress to the foot of the arch, i.e., above the coal pillars on both sides of the goaf. Consequently, stress was concentrated in the coal pillars on both sides of the goaf. The overburden damage in the strip working face is shown in Figure 6.

After the strip working face was mined, the overlying rock in the strip quarry area moved and a large subsidence occurred. The rock sank in the left and right sides of the strip quarry zones to a depth of 2.1 and 2.4 m, respectively (measurement line BG). However, the rock seam above the riser fracture zone underwent less subsidence. This suggests that because the strip mining was extremely inadequate (the width-to-depth ratio was

approximately 1/11) and the coal pillar left in the strip was relatively wide (the strip extraction rate was only 33.3%), the overburden rock movement in the strip working face was better controlled, and the overburden rock and surface subsidence were extremely slight. Figure 7 shows the overburden subsidence curves monitored by each measurement point after the strip working face was mined.

Figure 6. Overburden failure of strip mining.

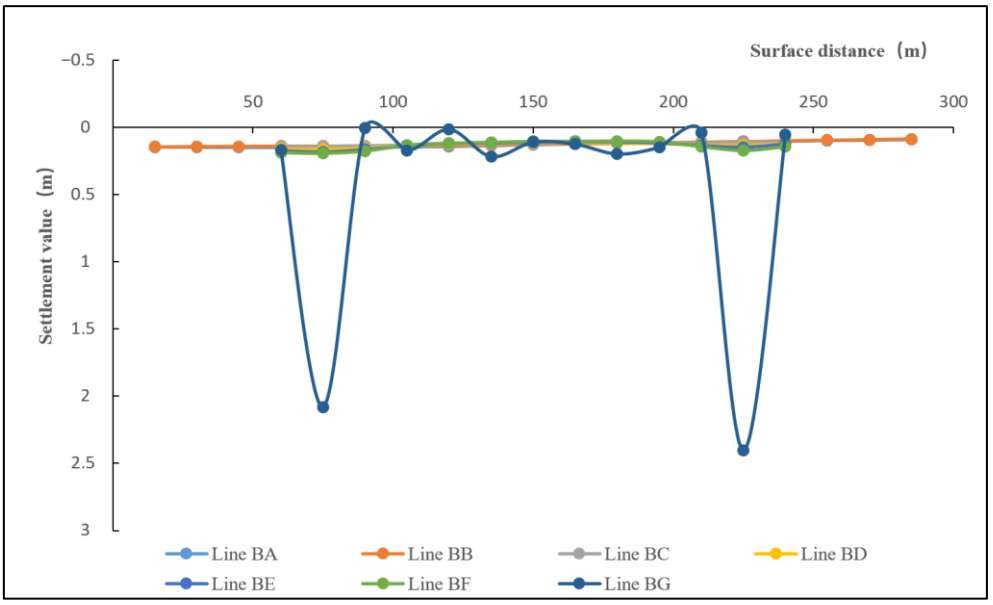

Figure 7. Overburden subsidence curves of strip mining.

4.2. Activation and Evolution of Overburden Rock Affected by Water Immersion in the Strip Goaf

After the strip was mined, the model was sealed. The sealing procedure involved the use of a transparent plexiglass plate to seal the front and back of the model frame. Water-stop sealing rubber strips were pressed onto the left and right sides and bottom of the plexiglass plate during installation. The model also applied expanding water-stop glue to the areas on both sides and the bottom of the simulated rock and soil that were not affected by mining to ensure sealing. The model sealing effect is shown in Figure 8. Subsequently, water was injected into the goaf to fill the entire strip-shaped cracking area, and the phenomenon of activation movement of the overlying rock affected by water immersion in the strip goaf was continuously observed.

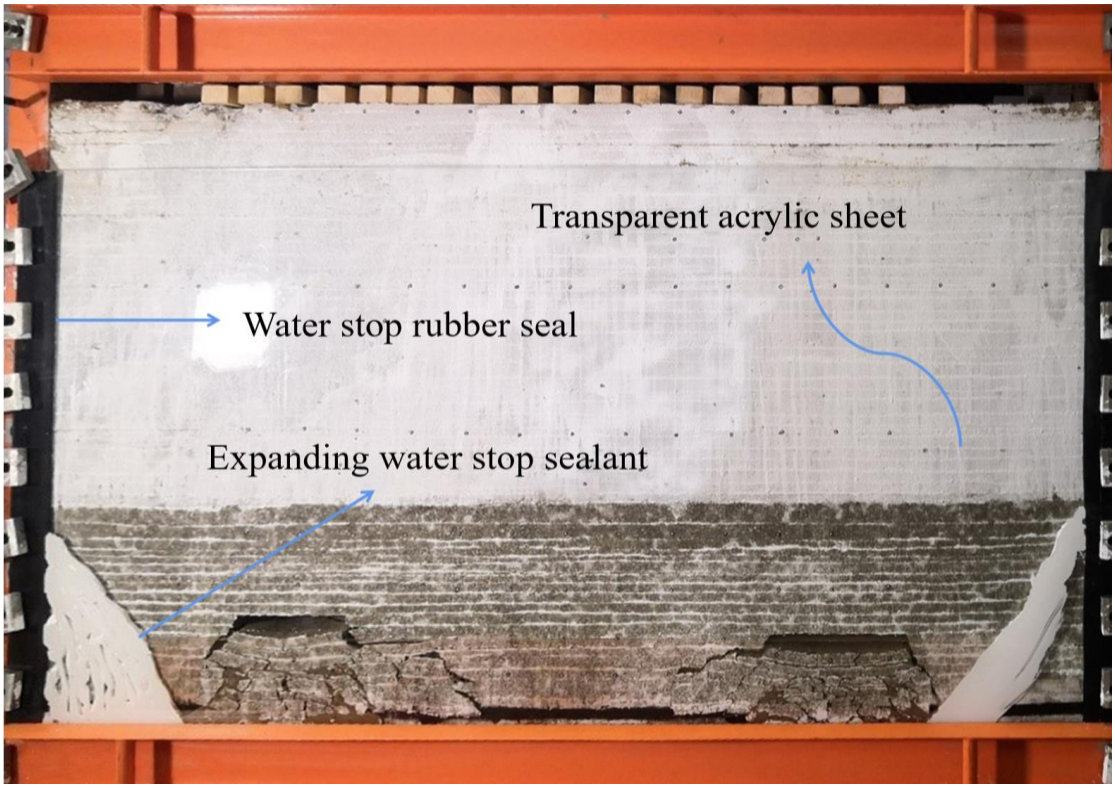

Figure 8. Model sealing effect.

Following the accumulation of water in the strip goaf, the mechanical strength of the collapsed rock and coal (rock) pillar was reduced. The stable surrounding rock in the strip goaf moved again, and the equilibrium structure of the overlying rock body was destroyed owing to the occurrence of activation. Consequently, with the continuous accumulation of water in the goaf and the extended water immersion time of the coal (rock) pillar, the activation failure characteristics of the overlying rock in the strip goaf exhibited characteristics that can be divided into two stages:

(1) Coal pillar corrosion stage

After strip mining, the overlying rock collapsed and filled the goaf, and there were still more holes, fissures, and other spaces in the strip goaf. Thus, water from the roof aquifer slowly seeped (or rushed) into the strip goaf, resulting in water accumulation. Under the immersion effect of water, the broken rock blocks in the goaf were continuously softened and compacted. The cracked rock blocks then failed to support the overlying rock layer, and the stress arch above the cracked zone further transferred the self-weight load of the overlying rock above to the coal pillar on both sides of the goaf. This further concentrated the stress of the coal pillar on both sides of the goaf. At the same time, the mechanical strength of both sides of the coal pillar gradually deteriorated and creep

occurred under the action of water immersion, until shear damage occurred at the edge of the coal pillar. This resulted in further expansion and development of the fracture in the strip goaf and small step subsidence of the overlying rock above the fracture zone. With further water immersion in the strip goaf, the strip coal pillar underwent shear damage from outside to inside several times, and the overburden rock underwent step subsidence numerous times. The evolution of overburden damage in the coal pillar corrosion stage under the action of water immersion in the goaf is shown in Figure 9.

Figure 10 shows the subsidence curve of overburden at one measurement point (BE12) above the strip goaf on the right side of the model. Evidently, at this stage, four instances of shear damage occurred in the strip coal pillar: 0.073, 0.132, 0.195, and 0.242 m.

(2) Coal pillar destabilization stage

Under the continuous immersion of water in the coal pillar, shear failure occurred on both sides of the coal pillar from the outside to the inside. The width of the core area of the coal pillar gradually decreased until it was inadequate to support the load weight of the overlying rock. Overall instability failure occurred, and the strips on both sides were connected to each other, forming a saddle-like overall cracking zone (Figure 11). The overlying rocks underwent large overall subsidence, forming a subsidence basin with a large middle and small sides (Figure 12). The subsidence at measurement point BE12 in the overburden changed abruptly from 0.30 to 1.63 m (Figure 10); subsequently, the increment of overburden subsidence leveled off with time.

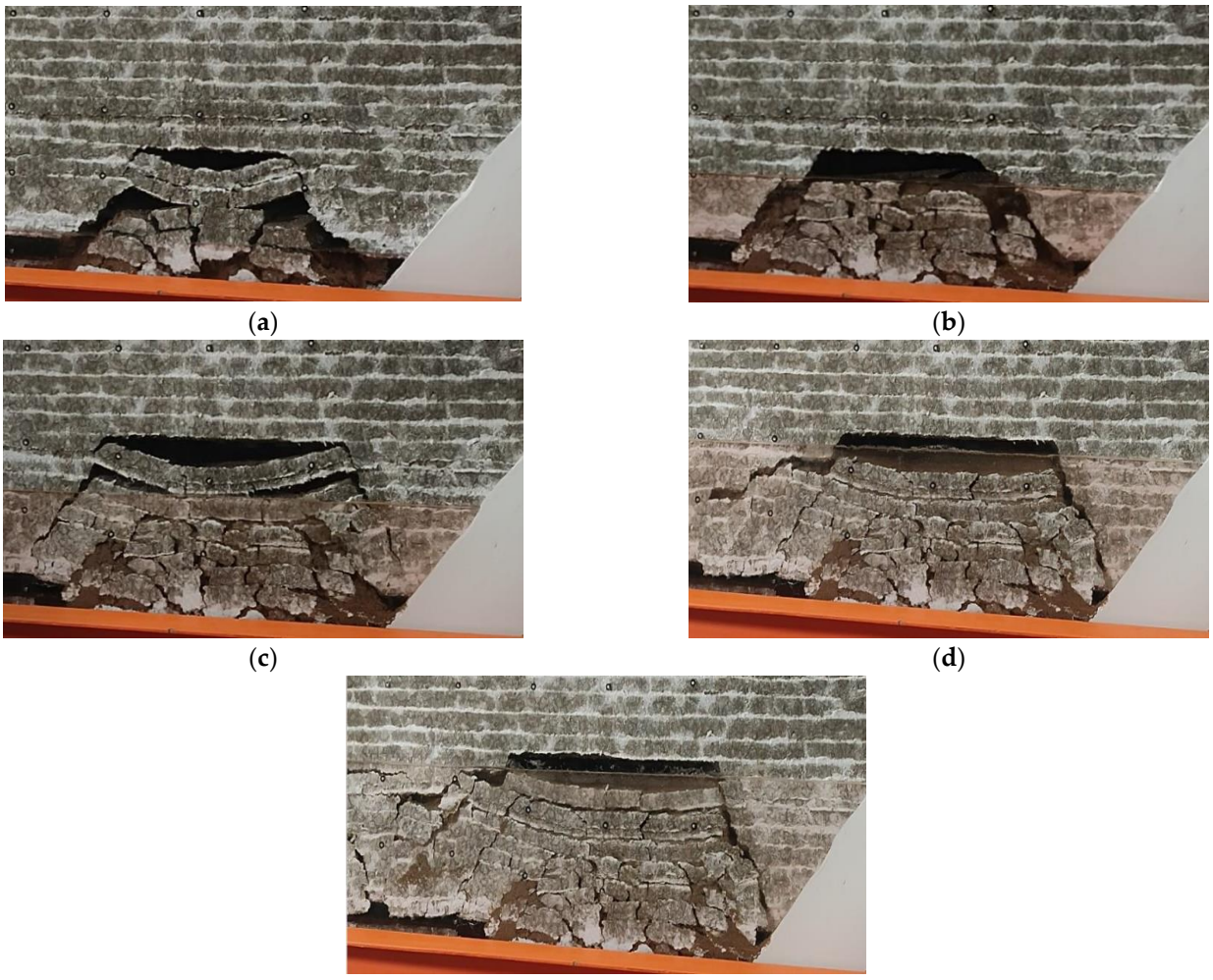

(**a**) (**b**) (**c**) (**d**) (**e**)

Figure 9. Evolution of overburden destruction on the right side in coal pillar corrosion stage affected by water immersion in the strip goaf. (**a**) Water starts to inrush in goaf. (**b**–**e**) First, second, third, and fourth instances of shear damage of coal pillar, respectively.

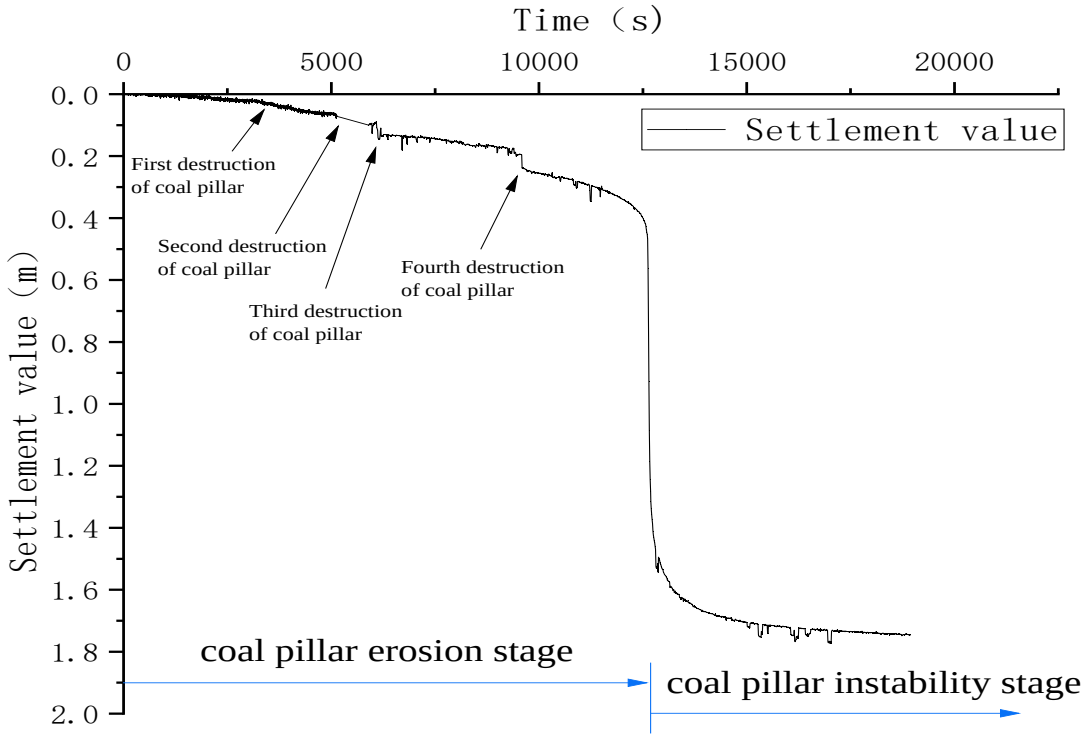

Figure 10. Dynamic subsidence curve of measurement point BE12 with time of water immersion in goaf.

Figure 11. Overburden damage pattern of coal pillar destabilization affected by water immersion in the strip goaf.

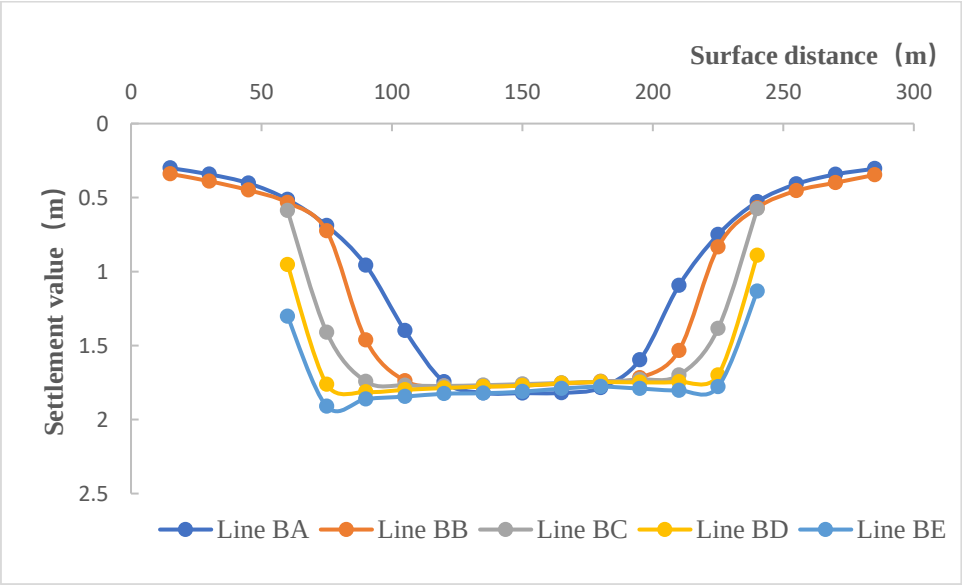

Figure 12. Overburden subsidence curve of strip coal pillar instability affected by water immersion in the strip goaf.

From 10 September 2018 to 23 February 2019, a geological drilling rig was used at Dai Zhuang Coal Mine to conduct core exploration of the mining area. For verification of the mining area exploration, 14 holes were drilled, including 6 holes to expose the mining area and 8 holes for the coal pillar. For coal pillar drill holes, the average bulk density of a normal coal seam is 1.388 g/cm^3, and the coal pillar is disturbed by the mining area after the fissure increases. According to the actual measurement of the coal pillar drill holes, the void rate was 8.00% at 10 m distance from the mining area, 7.64% at 15.5 m distance, and 2.09% at 26.6 m distance. Based on the degree of void ratio reduction, the analysis found that the coal pillar was affected by the mining void area up to 20 m on both sides of that area, indicating that the coal pillar was damaged by the joint action of water infiltration pressure and top plate mine pressure in that area for many years after mining, confirming the damage characteristics of the coal pillar reflected by the physical simulation test in the erosion stage.

5. Mechanism of Strip Coal Pillar Destabilization under the Action of Water Immersion

5.1. Coal Pillar Stability Evaluation Method

(1) Load on the strip coal pillar

According to an assumption by Wilson [33], coal pillars are believed to bear the weight of the overlying rock and share its weight in the goaf (see Figure 13). Thus, the load on the strip coal pillar is as follows:

$$P = \gamma H[a + \frac{b_1}{4}(2H - \frac{b_1}{0.6}) + \frac{b_2}{4}(2H - \frac{b_2}{0.6})] \cdot L \quad (1)$$

In the formula, P is the coal pillar load (kg), γ is the average bulk density of the overlying rock (kg/m^3), H is the mining depth (m), a is the width of the strip coal pillar (m), b_1, b_2 represent the width of the strip-mining area on both sides (m), and L is the coal pillar length (m).

When the distance between b_1 and b_2 reaches 0.3H, the vertical stress of the goaf will return to the original load γH. At this time, the weight of the overlying stratum will not be completely borne by the coal pillar, and the rock falling into the goaf bears part of the overlying stratum. The calculation formula of coal pillar load P is as follows:

$$P = \gamma H[a + 0.3H] \cdot L \quad (2)$$

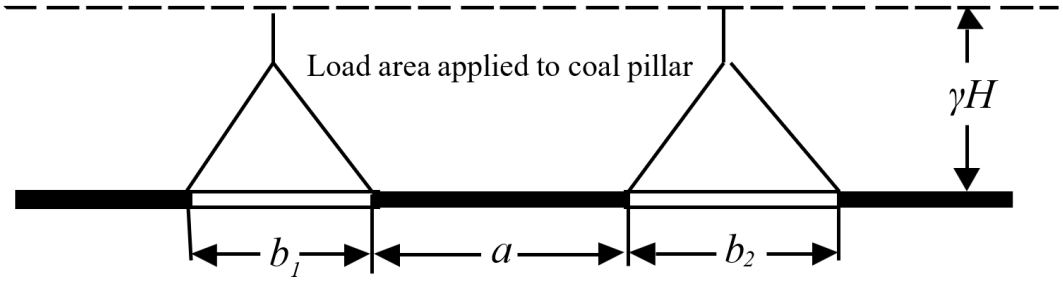

Figure 13. Wilson's coal pillar load calculation method.

(2) Bearing capacity of strip coal pillars

According to the hypothesis of Wilson (1970), a coal pillar is composed of elastic and plastic zones. The damaged plastic zone surrounds the elastic zone and forms a constraint on the elastic zone. Furthermore, the elastic zone is in a state of triaxial stress, which generally conforms to the law of elasticity. The stability limit of the coal pillar is the mean stress in the elastic zone $\bar{\sigma} = 4\gamma H$. Here, the coal pillar plastic zone width is $r_p = 0.00492\,HM$. Thus, the calculation formula for the bearing capacity of the strip coal pillar in the elastic zone is:

$$P_C = 4\gamma H(a - 4.92MH \times 10^{-3}) \cdot L \quad (3)$$

In the formula, P_C is the coal pillar bearing capacity (kg) and M is the coal pillar thickness (m).

(3) Coal pillar stability evaluation

Coal pillar safety factor n can be calculated as follows:

$$n = \frac{P_C}{P} \quad (4)$$

When $n \geq 1$ (i.e., $P_C \geq P$), the strip coal pillar can bear the load of the overlying stratum and remains stable.

When $n < 1$ (i.e., $P_C < P$), the strip coal pillar cannot bear the load of the overlying stratum and is unstable and causes damage.

5.2. Evolution Process of Coal Pillar Instability under the Action of Water Immersion

Figure 14 shows a schematic diagram of the creep destabilization evolution of the coal column under the action of water infiltration. After the groundwater infiltrates or surges into the mining area, the strip coal pillar will be subjected to the combined action of the infiltration pressure of the water and the top plate mineral pressure, and the water in the mining area will infiltrate into the plastic zone of the coal pillar through the fissures or pore spaces up to the elastic zone. Under the prolonged action of groundwater, the coal pillar will undergo creep deterioration and its strength will be continuously reduced. At the same time, as the plastic zone of the coal pillar is in the peak compressive stress state, the strength of the coal pillar is likely to be less than the compressive stress in the process of creep decay, and shear damage of the coal pillar in the plastic zone will occur. This will result in the overlying rock seam compressive zone shifting to the inner side of the coal pillar, and the plastic zone will also shift from outside to inside, shortening the elastic zone and weakening the bearing capacity of the coal pillar. In this way, the cycle of softening of the plastic zone of the coal pillar–destabilization of strength–inward movement is repeated, resulting in the elastic zone gradually shortening until the bearing capacity of the coal pillar cannot support the load, and the coal pillar will become unstable as a whole,

causing another large settlement of the overlying rock until the whole overlying rock reaches a new state of mechanical equilibrium.

The penetration depth in the elastic zone of the coal pillar is r_f. Coal rock exhibits strong creep characteristics [34], and fissures or pore water softens the coal rock mass and reduces the creep threshold stress and creep strength of coal rock [35–39]. Studies have shown that the creep strength of coal rock after immersion decreases with time, its long-term strength tends to reach a certain value, and its creep strength can be fitted with an exponential function [40]:

$$\sigma_{cr} = \sigma_{\infty} + Aexp(-Bt) \quad (5)$$

In the formula, σ_{cr} is the creep strength of coal rock after immersion in water (MPa), σ_{∞} is the ultimate strength of coal rock creep (MPa), A is the coal rock attenuation strength (MPa), and B is the attenuation coefficient (d).

The creep strength of water-soaked coal and rock continues to weaken with time. Simultaneously, the mine pressure in the open area of the coal pillar is in a state of peak stress. If $\sigma_{\infty} < k\gamma H$ (k is the peak stress concentration factor), the coal rock strength is attenuated during the creep. There is a risk of creep damage in the hollow area on either side of the coal pillar, which results in shortening of the elastic zone of the coal pillar and weakening of the bearing capacity:

$$P_C = 4\gamma H(a - r_{f1} - r_{f2} - 4.92MH \times 10^{-3}) \cdot L \quad (6)$$

Under the combined action of osmotic pressure and water immersion softening, stagnant water further penetrates and expands into the elastic zone of the coal pillar, and the damage area will extend toward the middle, thus forming a vicious circle. This leads to further shortening of the elastic zone of the coal pillar until the load-carrying capacity P_C of the pillar is less than the load carried P, and the pillar will become unstable as a whole.

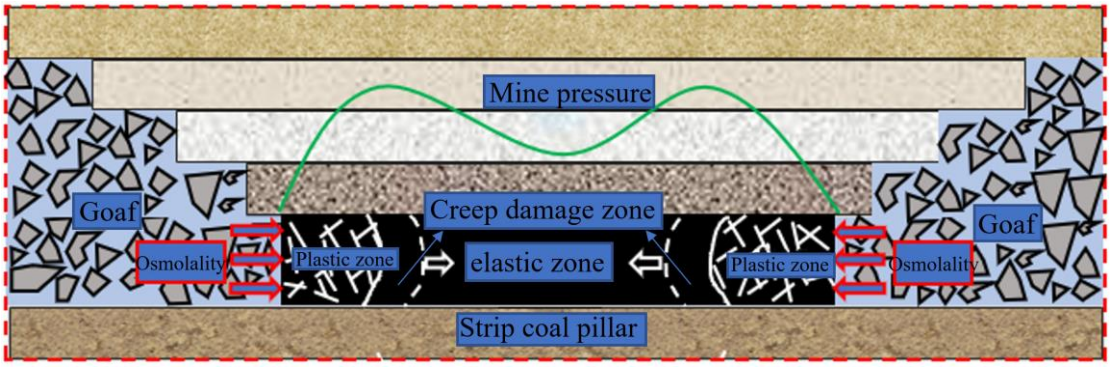

Figure 14. Schematic diagram of creep instability evolution of coal pillar under the action of water immersion.

6. Conclusions

In this study, the evolution of residual coal and rock columns in a strip-mining area under the action of water immersion was analyzed by means of similar material simulation tests, and the variation in the overburden damage characteristics and sinkage amount over time with water accumulation in the mining area was summarized, revealing the destabilization mechanism of coal columns in the strip under the action of water immersion. The following main conclusions were drawn:

(1) After water accumulated in the strip goaf, the instability evolution process of the strip coal pillar could be divided into stages over time. In the early stage of erosion, the mechanical strength on both sides of the coal pillar gradually deteriorated and crept under the action of water immersion, and the edge of the coal pillar suffered multiple shear failures. In the later stage of overall instability, owing to multiple creep failures from the outside to the inside on both sides of the coal pillar, the width of the elastic region gradually

shortened until it was inadequate to support the load weight of the overlying strata and there was overall instability failure.

(2) The overlying rock failure and subsidence in the strip goaf exhibited characteristics that could be divided into stages with the evolution of instability of the strip coal pillar. In the erosion stage, with gradual creep failure of the strip coal pillar, the cracking height of the overlying rock in the strip goaf gradually expanded and developed upward, and the overlying rock exhibited small step subsidence several times. During the overall instability stage, owing to the overall instability and failure of the strip coal pillar, the goaf was connected on both sides of the strip, and the overlying rock underwent a sudden large subsidence.

(3) Under the action of water infiltration pressure in the mining area, water crept into the coal rock hollow area, its strength decreased with time, and its long-term strength tended to reach a certain value. When the value was less than the overlying mine pressure value, the coal rock strength in the creep decay process, the hollow area creep damage, and the coal pillar elastic zone were reduced, forming a vicious cycle. The damaged area continued to expand to the middle and the coal pillar elastic zone was constantly shortened, finally leading to lower coal pillar bearing capacity. This reveals the mechanism of coal pillar instability in the strip under the action of water immersion in the mining area.

The conclusions of this study were mainly obtained from physical simulation tests. As the destructive effect of water accumulation on coal pillars in mining areas is a very long evolutionary process, the experimental research site is not yet able to effectively support these conclusions due to the relatively short formation time of the mining area and the limited observation data. However, similar material simulation tests carried out in this study strictly followed the similar theory and are finely produced, and the final phenomena reflected by the tests are reasonable; therefore, the research results are still of certain theoretical guidance significance for guiding the study of coal pillar stability under the action of groundwater.

Author Contributions: Conceptualization, formal analysis, resources, writing—review and editing, S.Y.; Writing—original draft, data curation, formal analysis, Y.Z.; Formal analysis, methodology, project administration, H.Y.; Project administration, validation, supervision, X.L.; Software, data curation, X.W.; Visualization, translation, Y.W. Writing—review and editing, T.C. All authors have read and agreed to the published version of the manuscript.

Funding: The research was sponsored by grants from the National Natural Science Foundation of China (Nos. 51974125, 52274199) and the National Natural Science Foundation of China Youth Science Fund Project (No. 52004090).

Institutional Review Board Statement: Not applicable.

Informed Consent Statement: Not applicable.

Data Availability Statement: The data presented in this study are available on request from the corresponding author.

Acknowledgments: The authors thank the reviewers for their valuable comments and careful reading of the manuscript.

Conflicts of Interest: The authors declare no conflict of interest.

References

1. Yan, Z.; Shi, S.; Dang, B.; Liu, C.; Xu, T. Research on the Failure Mechanisms of Rock Masses under Level Seismic Loading. *China Earthq. Eng. J.* **2013**, *2*, 5–9.
2. Cao, A.; Fan, J.; Mou, Z.; Guo, X. Burst failure effect of mining-induced tremor on roadway surrounding rock. *J. China Coal Society* **2010**, *35*, 60–64.
3. Yi, X.; Zhengzheng, C.; Zhenhua, L. Destabilization mechanism and energy evolution of coal pillar in rockburst disaster. *Arab. J.Geosci.* **2020**,*13*.DOI: 10.1007/s12517-020-05584-4.
4. Maleki, H. Coal pillar mechanics of violent failure in U.S. Mines. *Int. J. Min. Sci.Technol.* **2017**, *27*, 387–392.

5. Deng, J.; Kanwar, N.S.; Pandey, M.D.; Xie, W.C. Dynamic buckling mechanism of pillar rockbursts induced by stress waves. *J. Rock Mech. Geotech. Eng.* **2019**, *11*, 944–953.
6. Xia, Z.; Yao, Q.; Meng, G.; Xu, Q.; Tang, C.; Zhu, L.; Wang, W.; Shen, Q. Numerical study of stability of mining roadways with 6.0-m section coal pillars under influence of repeated mining. *Int. J. Rock Mech. Min. Sci.* **2021**, *138*, 104641.
7. Rashed, G.; Slaker, B.; Murphy, M. Exploration of Limestone Pillar Stability in Multiple-Level Mining Conditions Using Numerical Models. *Min. Metall. Explor.* **2022**, 2524–3462. DOI: 10.1007/s42461-022-00655-4.
8. Lan, H.; Han, K.; Han, Z. Surface residual subsidence and coal pillar stability influenced by coal creep in deep strip mining. *J. China Coal Soc.* **2022**. DOI:10.13225/j.cnki.jccs.2021.1853.
9. Teng, Y.; Tang, Z.; Yi, S.; Yan, C. Evaluation of foundation stability in coal mine subsidence area and deformation resistance technology. In Proceedings of the 25th International Conference on Geoinformatics Buffalor, NY, USA, 2–4 August 2017.
10. Zhu, X.; Guom, G.; Liu, H.; Peng, X.; Yang, X.Research on the Stability Evaluation Model of Composite Support Pillar in Backfill-Strip Mining. *Math. Probl. Eng.* **2020**, *2020*. DOI: 10.1155/2020/3138258.
11. Bin, L.I.; Deng, K.Z.; Niu, H.P. Evaluation on Stability of Foundation above Old Mining Goaf. *Coal Eng.* **2012**, *111*, 21–26.
12. Han, P.; Zhang, C.; Wang, W. Failure analysis of coal pillars and gateroads in longwall faces under the mining-water invasion coupling effect. *Eng. Fail. Anal.* **2022**, *131*, 105912.
13. Ai, T.; Wu, S.; Zhang, R.; Gao, M.; Zhou, J.; Xie, J.; Ren, L.; Zhang, Z. Changes in the structure and mechanical properties of a typical coal induced by water immersion. *Int. J. Rock Mech. Min. Sci.* **2021**, *138*, 104597.
14. Yao, Q.; Chen, T.; Ju, M.; Liang, S.; Liu, Y.; Li, X. Effects of Water Intrusion on Mechanical Properties of and Crack Propagation in Coal. *Rock Mech. Rock Eng.* **2016**, *49*, 4699–4709.
15. Li, G.; Wang, Z.; Ma, F.; Guo, J.; Liu, J.; Song, Y. A Case Study on Deformation Failure Characteristics of Overlying Strata and Critical Mining Upper Limit in Submarine Mining. *Water* **2022**, *14*, 2465.
16. Zhou, Q.L.; Liu, D.P.; Lin, X.D. Pre-evaluation of fault stability for underground mining based on geomechanical fault-slip analysis. *Geomat. Nat. Hazards Risk* **2022**, *13*, 400–413.
17. Kai, W.; Guorui, F.; Jinwen, B.; Jun, G.; Xudong, S.; Boqiang, C.; Cheng, S. Dynamic behaviour and failure mechanism of coal subjected to coupled water-static-dynamic loads. *Soil Dyn. Earthq.Eng.* **2022**, *153*, 107084.
18. Poulsen, B.A.; Shen, B.; Williams, D.J.; Huddlestone-Holmes, C.; Erarslan, N.; Qin, J.Strength reduction on saturation of coal and coal measures rocks with implications for coal pillar strength. *Int. J. Rock Mech. Min. Sci.* **2014**, *71*, 41–52.
19. Dai, J.; Shan, P.; Zhou, Q. Study on Intelligent Identification Method of Coal Pillar Stability in Fully Mechanized Caving Face of Thick Coal Seam. *Energies* **2020**, *13*, 305.
20. Castellanza, R.; Gerolymatou, E.R. Nova. An Attempt to Predict the Failure Time of Abandoned Mine Pillars. *Rock Mech. Rock Eng.* **2008**, *41*, 377–401.
21. Frith, R.; Reed, G. Limitations and potential design risks when applying empirically derived coal pillar strength equations to real-life mine stability problems. *Int. J. Min. Sci. Technol.* **2019**, *29*, 17–25.
22. Kumar, R.; Das, A.J.; Mandal, P.K.; Bhattacharjee, R.; Tewari, S. Probabilistic stability analysis of failed and stable cases of coal pillars. *Int. J. Rock Mech. Min. Sci.* **2021**, *144*, 104810.
23. Li, H.; Guo, G.; Zha, J.; He, Y.; Wang, Z.; Qin, S. Stability evaluation method for hyperbolic coal pillars under the coupling effects of high temperature and ground stress. *Environ. Earth Sci.* **2017**, *76*, 704.
24. Chen, Sh.; Guo, We.; Zhou, H.; Shen, B.; Liu, J. Field investigation of long-term bearing capacity of strip coal pillars. *Int. J. Rock Mech. Min. Sci.* **2014**, *70*, 109–114.
25. Liu, S.; Wan, Z.; Zhang, Y.; Lu, S.; Ta, X.; Wu, Z. Research on evaluation and control technology of coal pillar stability based on the fracture digitization method. *Measurement* **2020**, *158*, 107713.
26. Xiao, T.; Jianbiao, B.; Lei, X.; Xuebin, Z. Characteristics of stress distribution in floor strata and control of roadway stability under coal pillars. *Min. Sci. Technol.* **2021**, *21*, 243–247.
27. Zhang, C.; Zhao, Y.; Han, P.; Bai, Q. Coal pillar failure analysis and instability evaluation methods: A short review and prospect. *Eng. Fail. Anal.* **2022**, *138*, 106344.
28. Guy, R.; Kent, M.; Russell, F. An assessment of coal pillar system stability criteria based on a mechanistic evaluation of the interaction between coal pillars and the overburden. *Int. J. Min. Sci. Technol.* **2017**, *27*,9–15.
29. Jiang, S.; Fan, G.; Li, Q.; Zhang, S.; Chen, L. Effect of mining parameters on surface deformation and coal pillar stability under customized shortwall mining of deep extra-thick coal seams. *Energy Rep.* **2021**, *7*, 2138–2154.
30. Wenbing, G.; Feiya, X. Numerical simulation of overburden and surface movements for Wongawilli strip pillar mining. *Int. J. Min. Sci. Technol.* **2016**, *26*, 71–76.
31. Wang, F.; Liang, N.; Li, G. Damage and Failure Evolution Mechanism for Coal Pillar Dams Affected by Water Immersion in Underground Reservoirs. *Geofluids* **2019**, *2019*,1–12.
32. He, G.; Yang, L.; Ling, G.; Jia, F.; Hong, D. Mining Subsidence Science .China University of Mining and Technology press,1991.
33. Wu Lixin,Wang Jinzhuang.Calculation of width of yielding zone of coal pillar and analysis of influencing factors .*J. China Coal Soc* **1995**, *20*, 625–631.
34. Danesh, N.N.; Chen, Z.; Aminossadati, S.M.; Kizil, M.; Pan, Z.; Connel, L.D. Creep: A Neglected Phenomenon in Coal Permeability Evolution and Coalbed Methane Production. In *SPE Asia Pacific Unconventional Resources Conference and Exhibition*; Brisbane , Australia ,2015.

35. He, F.; Meng, F.; Wang, Z; Zhao, G. Experimental research of water and coal(rock) creep. *J. Liaoning Tech. Univ.* **2011**, *30*, 175–177.
36. He,F.;Jia,Y.;Tai,Y. Experimental study on creep-seepage peak after crushing coal. *J. Liaoning Tech. Univ.* **2015**, 34, 999-1003.
37. Sainoki, A.; Mitri, H.S. Numerical investigation into pillar failure induced by time-dependent skin degradation. *Int. J. Min. Sci. Technol.* **2017**, *27*, 591–597.
38. Tingting, C.; Zengchao, F.; Yulong, J.; Dong, Z..; Dong, Z.; Xiaoqiang, Z. Seepage evolution in coal creep under different temperatures and different stresses. *Chin. J. Rock Mech. Engineering* **2018**, *37*, 101–107.
39. Yu, Y.; Chen, S.E.; Deng, K.Z.; Fan, D.H. Long-Term Stability Evaluation and Pillar Design Criterion for Room-and-Pillar Mines. *Energies* **2017**, *10*, 1644.
40. Chen, S.J.; Guo, W.J.; Yang, Y.J.; Wang, Y.B. Research on stability of strip coal pillar based on laboratory test. *Rock Soil Mechanics* **2008**, *29*, 2678–2682.